Magnetic and High-Frequency Dielectric Properties of Stuffed Pyrochlore Er_2TiO_5

A.B. Rinkevich*, D.V. Perov, E.A. Kuznetsov and M.S. Stenina

M.N. Mikheev Institute of Metal Physics Ural Branch of RAS, 18 S. Kovalevskaya St, Ekaterinburg, 620108 Russia

Abstract: The magnetic and high-frequency dielectric properties of a nanocomposite with particles of stuffed titanate pyrochlore Er_2TiO_5 were studied. Particles up to 60 nm in size are embedded in a matrix of artificial opal with SiO_2 spheres 260 nm in diameter. Magnetization curves were measured at temperatures from 2 to 70 K. Temperature dependences of magnetic susceptibility were measured in fields of 1 kOe and 0.1 kOe in the range from 2 to 300 K. The transmission and reflection coefficients for electromagnetic waves with frequencies from 26 to 38 GHz were measured. It was found that the imaginary part of the dielectric constant ε'' of the composite is small, $\varepsilon'' \approx 0.023$.

Keywords: Stuffed titanate pyrochlore, Temperature dependence of susceptibility, Curie-Weiss temperature, Microwave transmission and reflection coefficients, High-frequency complex dielectric constant.

1. INTRODUCTION

In recent years, the properties of stuffed titanate pyrochlore Er_2TiO_5 have been studied. Er_2TiO_5 typically crystallizes in a hexagonal or orthorhombic structure, depending on the synthesis conditions. A review of its structural state, phase stability regions and phase transformations is given in [1]. The titanate Er_2TiO_5 has several areas of practical application. Its photocatalytic properties have found the greatest use [2, 3]. It is also used in membrane pH sensors for bio-sensing applications [4]. The resistance of Er_2TiO_5 complex oxides to ion irradiation makes them suitable for use as ceramic molds for nuclear waste for the immobilization of actinides. [5]. TiO_2 nanoparticles doped with both Er^{3+} and Yb^{3+} exhibited excellent upconversion properties in optics [6]. In terms of electrical properties, erbium titanate Er_2TiO_5 belongs to the class of gate dielectrics, which can be used in capacitors [7] and, due to the high mobility of charge carriers under the influence of an electric field, in thin-film transistor devices [8].

Order–disorder structural transformations in highly imperfect fluorite-derived R_2TiO_5-based (R = Tm, Er) solid solutions have been discussed in [9]. The formation of nanocomposites based on lattice packings of SiO_2 nanospheres containing clusters of crystalline phases of titanium oxides (TiO_2 and TiO) and rare earth titanates of the composition R_2TiO_5 or $R_2Ti_2O_7$, where R is Er, Dy, Gd, Pr, Tb and Yb, in the interspherical cavities, is described in [10]. The optical, magnetic and dielectric properties of opal matrices with interspherical nanocavities filled with crystalline multiferroics, piezoelectric and ferroelectric materials, including Er_2TiO_5 nanoparticles, were studied in [11].

The magnetic properties of rare earth titanates R_2TiO_5 have not been sufficiently studied, although there is evidence that the effect of a magnetic field can improve the photocatalytic performance of complex oxides [12]. The magnetic properties of these stuffed titanates are mainly due to the Er^{3+} ions, whereas Ti^{4+} is a non-magnetic one. $Fe_3O_4@SiO_2@Er_2TiO_5$ core–shell nanoparticles are superparamagnetic [2]. A study of the temperature dependence of the susceptibility and magnetization curves of the titanate Ho_2TiO_5 showed that the magnetic properties of the stuffed pyrochlores depend on the local structure [13].

The magnetic and dielectric properties of erbium titanate nanocomposite Er_2TiO_5 are studied in this article. The composites were obtained by depositing Er_2TiO_5 nanoparticles into the interspherical volumes of an opal matrix. Magnetization curves and temperature dependences of magnetic susceptibility were measured, temperature ranges within which the Curie-Weiss law holds were established, and the Curie temperatures were determined. The complex permittivity was determined from the frequency dependences of the transmission and reflection coefficients of microwaves from a plate of nanocomposite Er_2TiO_5. These measurements were performed in the frequency range from 26 to 38 GHz. The structure and phase composition of the composites were studied.

2. PREPARATION OF SAMPLES AND CHARACTERIZATION

The crystalline structure of titanates of the R_2TiO_5 type has been studied in detail in [14]. Two structural modifications of Er_2TiO_5 are known: in an orthorhombic

*Address correspondence to this author at the M.N. Mikheev Institute of Metal Physics Ural Branch of RAS, 18 S. Kovalevskaya St, Ekaterinburg, 620108 Russia;
E-mail: rin@imp.uran.ru

Received on 01-06-2026 Accepted on 15-07-2026 Published on 21-07-2026

E-ISSN: 2410-4701/26

or hexagonal types of structure. The orthorhombic modification belongs to Space Group Cmcm and has the following lattice parameters: *a*= 5.842 Å; *b*= 5.842 Å; *c*= 10.451 Å. The characteristics of two crystalline forms of bulk Er_2TiO_5 samples are presented on the website [15]. It is stated there that this compound has no net magnetic moment. In [11], it is indicated that nanocomposite Er_2TiO_5 crystallizes in the hexagonal crystal system, Pbam, and has a pyrochlore structure.

Artificial opal matrices consisting of amorphous SiO_2 spheres with a diameter of approximately 260 nm were used as matrices for the composites. Nanocomposite samples were formed by repeatedly filling the opal matrices with solutions of $Er(NO_3)_3$ and $TiCl_3$ salts in HCl. After each impregnation, the samples were then held at a temperature of $T \approx$ 670–720 °C. A chemical reaction occurred, and erbium and titanium oxides precipitated. Impregnation was performed seven times to a large measure fill the interspherical voids. After impregnation, annealing was performed at 900 °C for 4 hours, during which time Er_2TiO_5 particles formed. The process of preparing nanocomposites based on opal matrices is described in detail in [11, 16].

Structure of composite with Er_2TiO_5 particles has been investigated with scanning electron microscope Tescan MIRA LMS. The image of structure produced in BSE regime at x418 000 magnification is shown in Figure **1**. This image is obtained with fresh cleavage of the sample. The ordered arrangement of submicron spheres as well as particles are clearly seen. Embedded particles are irregular in shape and their typical size is low than 60 nm. They are located in interspherical cavities, and due to the use of several impregnations, several particles can form in one cavity.

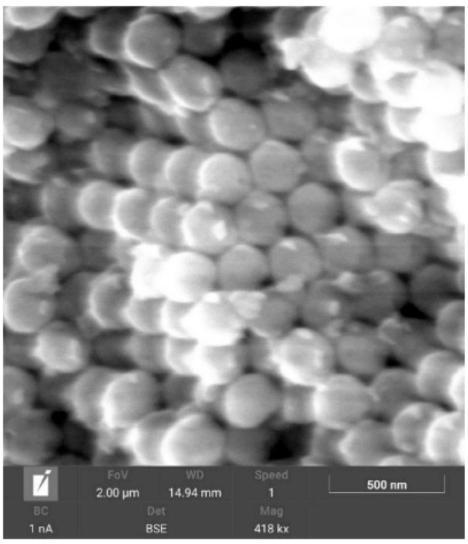

Figure 1: The structure of composite with Er_2TiO_5 particles obtained with scanning electron microscope Tescan MIRA LMS in BSE regime at magnification of 418 000.

The X-ray phase analysis of a composite sample with Er- and Ti-based compounds synthesized in nanovoids was carried out on an XRD-6000 X-ray diffractometer in CuK*α* radiation with a curved graphite monochromator. The analysis was performed without sample rotation, either in 0.02° increments or continuously at 1°/min. The X-ray diffraction pattern is shown in Figure **2**, and the data are presented in Table **1**. X-ray analysis allowed us to establish the following phases: mostly Er_2TiO_5 – hexagonal syngony and small amounts of $Ti_{0.72}O_2$ (anatase, synthetic) – tetragonal syngony, space group I41/amd and SiO_2 – monoclinic syngony, space group I2/a. The analysis performed by the EDAX system showed that the elemental composition of the sample corresponds to the nominal one. The volume of the introduced phase is about 7%. X-ray phase analysis showed that the composite does not contain other phases containing ions with a magnetic moment.

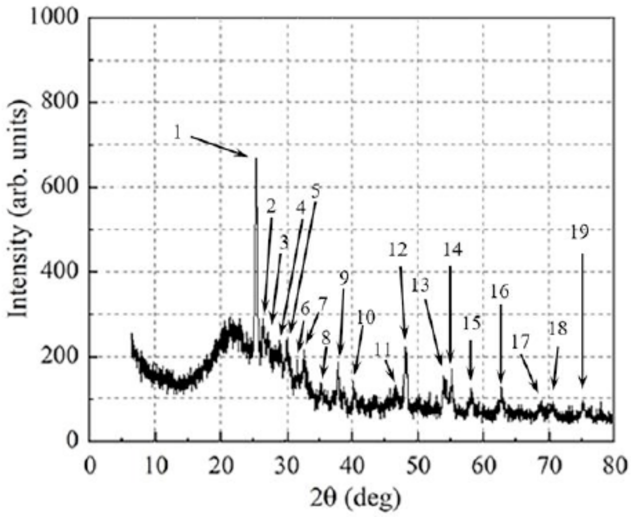

Figure 2: The X-ray diffraction image for the composite with Er_2TiO_5 particles obtained with XRD-6000 diffractometer.

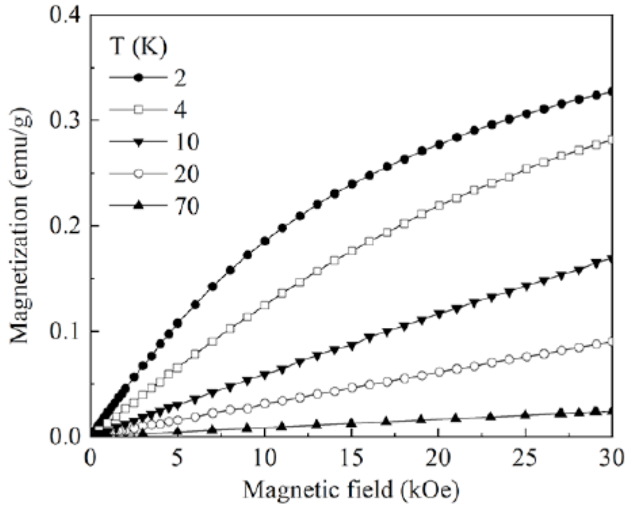

Figure 3: The magnetization curves for nanocomposite with Er_2TiO_5 particles measured at different temperatures.

Table 1: The X-Ray Data for the Composite

Peak's number	Experimental data					ICDD PDF-2 data: $Ti_{0.72}O_2$ (anatase, synthetic), SiO_2 and Er_2TiO_5								
	Intensity, arb. un.	Intensity, %	Bragg's angle 2*θ*, deg.	Peak half-width, deg.	Inter-planar spacing *d*, Å	$Ti_{0.72}O_2$ (anatase, synthetic) – tetragonal syngony, space group I41/amd			SiO_2 – monoclinic syngony, space group I2/a			Mostly Er_2TiO_5 – hexagonal syngony		
						d, Å	hkl	I, %	d, Å	hkl	I, %	d, Å	hkl	I, %
1	348	100.00	25.339	0.4039	3.5119	3.5144	101	100	3.4941	110	12			
2	106	30.46	26.400	0.6557	3.3731				3.3315	013	100			
3	82	23.56	27.140	0.3400	3.2828				3.2558	-112 004	15			
4	82	23.56	28.936	0.3216	3.0830							3.1080	100	30
5	75	21.55	29.995	0.5592	2.9765				2.9274	112	55	3.0060	101	
6	76	21.84	31.640	0.0262	2.8254									
7	57	16.38	32.600	0.2702	2.7444							2.7470	102	100
8	54	15.52	35.240	0.0831	2.5446				2.5484	-114	18			
9	69	19.83	37.800	0.3660	2.3779	2.3742	004	16						
10	69	19.83	40.060	0.0266	2.2488				2.2753	-121	7			
11	64	18.39	46.557	0.1000	1.9490				1.9509	123	29			
12	101	29.02	48.895	0.4780	1.8902	1.8915	200	26						
13	68	19.54	53.911	0.2671	1.6992	1.6975	105	16						
14	86	24.71	55.125	0.1833	1.6646	1.6656	211	13						
15	68	19.54	58.140	0.0274	1.5853				1.6097	033	11			
16	71	20.40	62.580	0.2063	1.4831	1.4794	204	9						
17	41	11.78	68.769	0.1691	1.3639	1.3622	116	5						
18	40	11.46	70.653	0.1391	1.3321	1.3375	220	5						
19	30	8.62	75.155	0.4516	1.2631	1.2633	215	8						

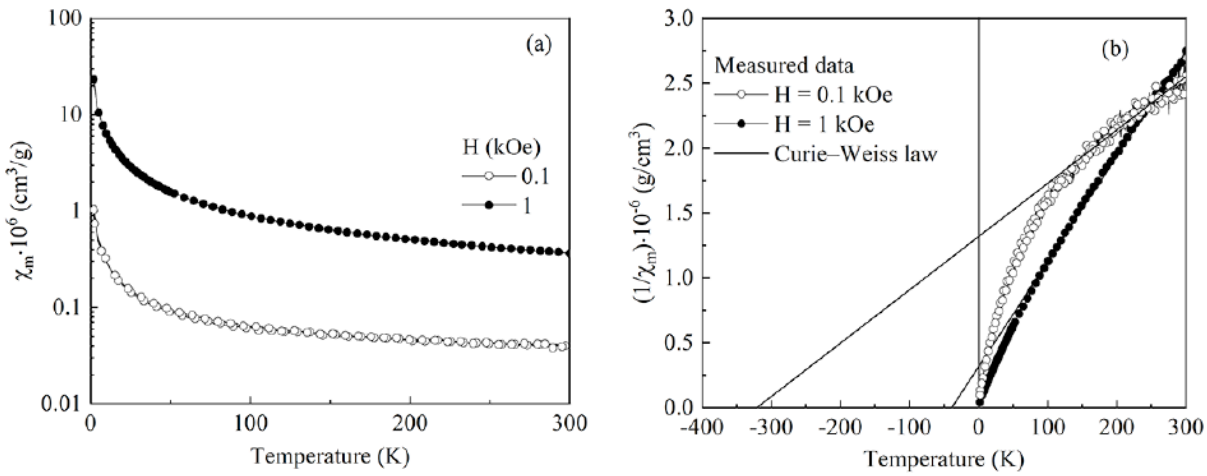

Figure 4: The temperature dependences of magnetic susceptibility (**a**) and inverse susceptibility (**b**) measured in the fields 1 kOe and 0.1 kOe.

3. MAGNETIC PROPERTIES

Measurements of the magnetic properties of the composites were carried out on a SQUID magnetometer MPMS-XL-5 at temperatures from 2 to 300 K. Magnetization curves and temperature dependences of magnetic susceptibility were measured. The results of measuring the magnetization curves at several temperatures are presented in Figure **3**. The dependence measured at a low temperature *T* = 2 K tends to saturate in fields *H* ~ 30 kOe. The magnetic saturation field is greater than 30 kOe. The dependences measured at temperatures above 10 K are close to linear. The high value of the saturation field is caused by the influence of the demagnetizing factor of titanate particles, which have a complex shape and are oriented differently relative to the external magnetic field. Figure **4a** shows the temperature dependences of the magnetic susceptibility $\chi(T)$, measured in fields of 1 kOe and 0.1 kOe. Susceptibility increases with decreasing temperature. These relationships are reversible, meaning they are virtually identical during cooling and heating. There is no temperature hysteresis in susceptibility. In the temperature range under consideration, the $\chi(T)$ dependence shows no features. It can be concluded that the spin glass state is not realized in Er_2TiO_5, as in Ho_2TiO_5 [13].

Figure **4b** shows the temperature dependences of the inverse susceptibility measured in fields of 1 kOe and 0.1 kOe. The dependence measured at 1 kOe is satisfactorily approximated by a linear dependence according to the Curie-Weiss law at temperatures above ~70 K

$$\chi_m = \frac{C}{T - \theta_{cw}}, \tag{1}$$

where θ_{cw} is the Curie temperature, and *C* is a constant. The dependence measured at 1 kOe corresponds to a Curie temperature of $\theta_{cw} \approx$ -39 K. The dependence measured in a field of 0.1 kOe can only be approximated by a linear dependence at high temperatures of 150–300 K. If we formally construct such an approximation, we obtain $\theta_{cw} \approx$ -321 K for the Curie temperature. Such a strong dependence of θ_{cw} on the temperature range and on the field strength in which the susceptibility was measured distinguishes the erbium titanate Er_2TiO_5 that we are considering from the holmium titanate Ho_2TiO_5 studied in [13]. In [17], data on the Curie temperature for erbium titanate-pyrochlore $Er_2Ti_2O_7$ are presented. Measurements in a field of 500 Oe in the range of 50-300 K gave the value θ_{cw} = -15.93 K, which differs significantly from the values we obtained for stuffed erbium titanate Er_2TiO_5. It is quite possible that the large value of θ_{cw} is associated with the presence of antiferromagnetic correlations. It is known [18] that in the case of stuffed spin ice titanate $Ho_{2+x}Ti_{2-x}O_{7-\delta}$ the quantum relaxation regime exists at $T > 1$ K, and in spin ice titanate $Ho_2Ti_2O_7$ a quantum relaxation regime persists to even *T* = 30–40 K.

Magnetic property measurements showed that the magnetic saturation field is quite high, while the composite's magnetization is low. It can be assumed that at temperatures above 150 K, the titanate enters a paramagnetic state. However, high Curie temperatures indicate the presence of strong magnetic correlations in the paramagnetic state. Figure **5** shows the temperature dependence of the temperature derivative of magnetic susceptibility. This dependence is calculated from the dependence shown in Figure **4a**, measured at *H* = 1 kOe. The dependence in Figure **5** is monotonic, without features that would indicate a phase transition. Thus, the spin glass state is not realized in the temperature range under consideration. However, it is possible that the transition occurs at a lower temperature. For example, in stuffed pyrochlore Ho_2TiO_5 the peak in capacitance at *T* = 1.6 K is obtained, suggesting that a longer-range ordering is occurring in this material [13].

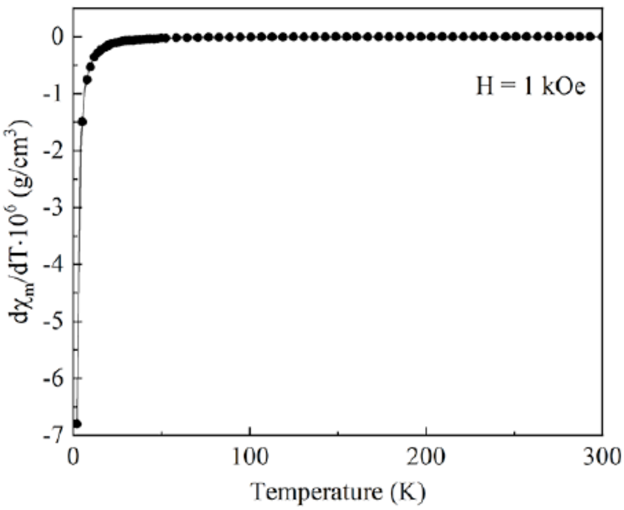

Figure 5: Monotonic temperature dependence of temperature derivative of magnetic susceptibility of the composite with Er_2TiO_5 particles.

Let us consider the temperature dependence of the product χT. As indicated in [19], this dependence allows for further analysis of the magnetic susceptibility, in addition to the usual procedure for studying the inverse susceptibility. The dependence χT as a function of *T* is constructed from the logarithm of *T*. In particular, this dependence in the paramagnetic region should have a horizontal plateau corresponding to the fulfillment of the Curie-Weiss law. The plateau must also be in the low-temperature region. The transition from a low-temperature plateau to a high-temperature plateau is called a Curie-law crossover. In the crossover region, the dependence χT of *T*, according to [19], can be approximated by the formula

$$\chi_m T = \frac{1 + b_1 \exp\left(\frac{c_1}{T}\right)}{a + b_2 \exp\left(\frac{c_2}{T}\right)}, \tag{2}$$

where a, b_1, b_2, c_1, c_2 are fitting coefficients. In Figure **6**, the circles correspond to the experimentally measured dependence. Its approximation using formula (2) is shown by the solid line.

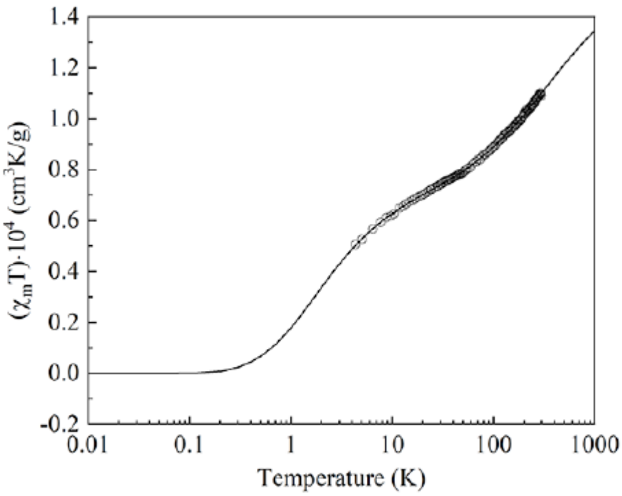

Figure 6: Temperature dependence of the product $\chi \cdot T$ and its approximation using formula (2). The symbols and solid line represent the experimental data and approximation respectively.

The approximation was carried out using the criterion of the minimum root-mean-square difference between the experimentally obtained dependence of the quantity and its approximation using expression (2) in the temperature range from $T_{\min}$ to $T_{\max}$ used:

$$\Delta = \frac{1}{T_{\max} - T_{\min}} \int_{T_{\min}}^{T_{\max}} \left[\left(\chi_m T\right) - \left(\chi_m T\right)_* \right]^2 dT . \quad (3)$$

The asterisk in expression (3) denotes the experimental dependence.

The values of the Curie constant and Curie temperature are determined by the relations

$$C = \frac{1 + b_1}{a + b_2} \quad (4)$$

and

$$\theta_{cw} = \frac{b_1 c_1}{1 + b_1} - \frac{b_2 c_2}{a + b_2} . \quad (5)$$

The approximation parameters and the results of determining *C* and θ_{cw} are given in Table **2**. As can be seen, the value of θ_{cw} found from the approximation differs significantly from that obtained from the inverse susceptibility analysis. According to [19], this means that the experiment did not reach the high-temperature limit corresponding to the full fulfillment of the Curie-Weiss law. The approximation results also show that the spin-liquid regime is not realized in the material under consideration. The most striking characteristic feature of the temperature dependence of magnetic susceptibility is the strong dependence of the Curie temperature on the magnetic field strength, which is associated with magnetic correlations in the paramagnetic state.

4. MICROWAVE PROPERTIES

Let's examine the results of measuring the microwave properties of the composite. The measurements were performed in the frequency range from 26 to 38 GHz using a scalar network analyzer. The sample was a 2 mm thick plate. It was placed in a rectangular waveguide with the cross section of 7.2 x 3.4 mm^2 such that it completely filled the waveguide's cross-section. The moduli of the transmission coefficient $|T|$ and reflection coefficient $|R|$ were measured. The frequency dependences of the coefficients $|T|$ and $|R|$ are shown in Figure **7a**.

This figure also shows the curves calculated for the frequency dependences of the coefficients using the method described in [20]. The permittivity was estimated within a sliding window of width ΔH = 0.25 GHz. After performing the evaluation, when the window was positioned at the lowest frequency in the range, the window was shifted by the value $\Delta H/2$ and the evaluation was performed again. After shifting the window across the entire frequency range, the real ε' and imaginary ε'' parts of the composite's permittivity were determined. The values of ε' and ε'' were chosen such that the difference between the calculated and measured transmission and reflection coefficients within the window was minimal in the least-squares sense.

The results of determining the permittivity, *i.e.* the frequency dependences ε' and ε'', are shown in Figure **7b**. Note that in the range under consideration, the frequency dispersion of permittivity is small. Table **3** shows the values of ε' and ε'', averaged over the entire frequency range of 26–38 GHz. The small value of the imaginary part of the composite's permittivity is noteworthy. This property of the composite may find practical application, since a small imaginary part of the permittivity means small losses of electrical power. The

Table 2: Fitting parameters for semi-log dependence of $\chi \cdot T$ on *T*

a, g/(cm^3·K)	*b$_1$*	*b$_2$*, g/(cm^3·K)	*c$_1$*, K	*c$_2$*, K	*C*, cm^3·K/g	θ_{cw}, K
-5.9947·10^4	-0.9834	6.0053·10^4	-2.7064	0.6255	1.5719·10^{-4}	-194.8427

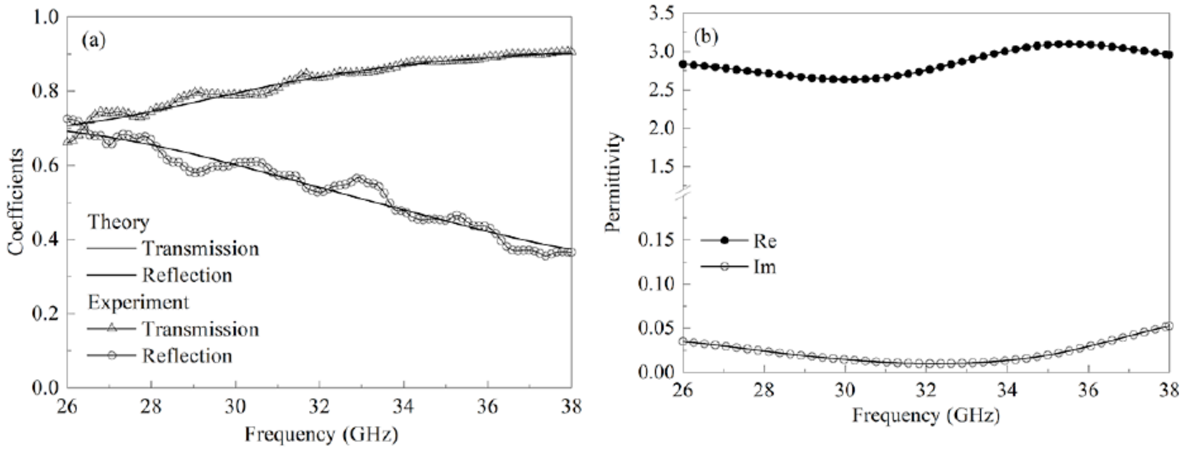

Figure 7: Measured and calculated frequency dependences of the moduli of transmission and reflection coefficients – (**a**); the frequency dependences of the real and imaginary parts of dielectric permittivity – (**b**).

small value is associated not only with the fact that the volume fraction of titanate particles in the composite is small and amounts to about 7%, but also with the following circumstance. It is possible that the very small value of ε'' for the composite based on the opal matrix is due to the fact that the opal contains grains whose size is comparable to the wavelength in the composite [21]. Therefore, during wave propagation, spatial dispersion is significant, which leads to a violation of the Kramers-Kronig dispersion relations. Violation of the dispersion relations can lead to a small value of ε'' [22, 23]. Unfortunately, there is currently limited information in the literature on the dielectric properties of erbium titanate Er2TiO5 and composites containing titanate particles. Information on the permittivity of composites based on opal matrices with spinel ferrite particles is provided in the article [24]. It was found that with a significant increase in heat treatment temperature, the matrix transitions to a ceramic state. This increases both the real and imaginary parts of the permittivity. In [7] the measurement of C-V curves at a frequency of 100 kHz was reported. In our nanocomposite titanate samples, measurements were performed at significantly higher frequencies of ~30 GHz. Small size of ε'' for composite can be used in microwave devices. Table **3** also shows the value of the effective microwave conductivity of the composite σ. The conductivity is introduced according to the expression $\varepsilon'' = \sigma / (\omega \varepsilon_0)$, where $\omega = 2\pi f$ is the circular frequency of the wave, ε_0 is the permittivity of vacuum.

Table 3: Mean dielectric permittivity and microwave conductivity

Frequency range, GHz	$\langle \varepsilon' \rangle$	$\langle \varepsilon'' \rangle$	$\langle \sigma \rangle$, S/m
26 - 38	2.74	0.023	0.041

5. CONCLUSIONS

Nanocomposites containing stuffed pyrochlore Er_2TiO_5 nanoparticles were synthesized. Scanning electron microscopy revealed that the matrix is an artificial crystal with SiO_2 microspheres approximately 260 nm in diameter. The inserted particles are located in the interspherical volumes. They have an irregular shape and dimensions less than 60 nm. The X-ray diffraction analysis revealed that the particles consist primarily of titanate Er_2TiO_5 and a small amount of $Ti_{0.72}O_2$ with an anatase structure.

Magnetization curves were measured at several temperatures in magnetic fields up to 30 kOe. The dependence measured at a low temperature of T = 2 K tends to saturate, and the magnetic saturation field is greater than 30 kOe. The dependences measured at temperatures above 10 K are close to linear. The temperature dependence of the inverse magnetic susceptibility, measured at 1 kOe, at temperatures above ~70 K is satisfactorily approximated by a linear dependence according to the Curie-Weiss law with a Curie temperature of $\theta_{cw} \approx$ -39 K. The dependence measured in a field of 0.1 kOe can only be approximated by a linear dependence at high temperatures of 150–300 K. If such an approximation is formally constructed, then for the Curie temperature we obtain $\theta_{cw} \approx$ -321 K. At temperatures above 150 K, the titanate undergoes a paramagnetic state. However, high Curie temperatures indicate the presence of magnetic correlations in the paramagnetic state. In the temperature range under consideration, from 2 to 300 K, the spin glass state is not realized.

The microwave properties of the composite were studied in the frequency range from 26 to 38 GHz at room temperature. The frequency dependences of the real (ε') and imaginary (ε'') parts of the permittivity were obtained. In the considered frequency range, the permittivity dispersion is small. The averaged value of the imaginary part of permeability over the entire frequency range is small, $\langle \varepsilon'' \rangle$ = 0.023 that can find out applications in microwave devices. Weak frequency dispersion of the real part of permittivity shows that useful microwave properties can be used beyond the 26–38 GHz frequency range. In future studies, it will be of interest to compare the dielectric properties of bulk and nanocomposite titanate over a wide frequency range.

FUNDING

The work was carried out within the framework of the state assignment of the Ministry of Science and Higher Education of the Russian Federation for the IMP UB RAS.

ACKNOWLEDGMENTS

The structure of nanocomposites was studied with scanning electron microscope Tescan MIRA LMS and magnetic measurements were performed with SQUID Magnetometer MPMS-XL-5 at the Collaborative Access Center "Testing Center of Nanotechnology and Advanced Materials" of the IMP UB RAS.

AUTHOR'S CONTRIBUTION STATEMENT

A.B. Rinkevich: Conceptualization, Methodology, Validation, Formal analysis, In-vestigation, Writing - Review & Editing. D.V. Perov: Investigation, Formal Analysis. E.A.Kuznetsov: Methodology, Investigation. M.S. Stenina: Resources, Investigation, Data curation.

CONFLICTS OF INTEREST STATEMENT

The authors declared no conflicts of interest.

REFERENCES

[1] G.R. Lumpkin, R.D. Aughterson, Perspectives on pyrochlores, defect fluorites, and related compounds: Building blocks for chemical diversity and functionality, Front. Chem. 9 (2021) 778140. https://doi.org/10.3389/fchem.2021.778140

[2] F. Gandomi, A. Sobhani-Nasab, S. Pourmasoud, M. Eghbali-Arani, M. Rahimi-Nasrabadi, Synthesis of novel Fe_3O_4@SiO_2@Er_2TiO_5 superparamagnetic core-shell and evaluation of their photocatalytic capacity, J. Mater. Sci.: Mater. Electron. 31 (2020) 10553-10563. https://doi.org/10.1007/s10854-020-03604-3

[3] M. Nazeri, H. Sedaghat, R. Rafiei, M.A. Farzin, S.M. Hosseinpour Mashkani, Er_2TiO_5@Ag nanocomposites: Enhanced photocatalysis and bacteria inactivation, and cytotoxicity, J. Rare Earths. 42 (2024) 851-858. https://doi.org/10.1016/j.jre.2023.10.017

[4] T.-M. Pan, P.-Y. Liao, K.-Y. Chang, L. Chi, Structural and sensing characteristics of $Gd_2Ti_2O_7$, Er_2TiO_5 and $Lu_2Ti_2O_7$ sensing membrane electrolyte-insulator-semiconductor for bio-sensing applications, Electrochim. Acta. 89 (2013) 798-806. https://doi.org/10.1016/j.electacta.2012.10.099

[5] R.D. Aughterson, G.R. Lumpkin, K.L. Smith, M. de los Reyes, J. Davis, M. Avdeev, M.C. Ridgway, J.M. Cairney, The ion-irradiation tolerance of the pyrochlore to fluorite $Ho_{(x)}Yb_{(2-x)}TiO_5$ and Er_2TiO_5 compounds: A TEM comparative study using both in-situ and bulk ex-situ irradiation approaches, J. Nucl. Mater. 507 (2018) 316-326. https://doi.org/10.1016/j.jnucmat.2018.05.026

[6] F. Trabelsi, F. Mercier, E. Blanquet, A. Crisci, R. Salhi, Synthesis of upconversion TiO_2:Er^{3+}-Yb^{3+} nanoparticles and deposition of thin films by spin coating technique, Ceram. Int. 46 (2020), 28183-28192. https://doi.org/10.1016/j.ceramint.2020.07.317

[7] T.M. Pan, W.H. Shu, J.L. Hong, Structural and electrical characteristics of Er_2TiO_5 gate dielectrics, Appl. Phys. Lett. 90 (2007) 222906. https://doi.org/10.1063/1.2744486

[8] F.H. Chen, J.L. Her, Y.H. Shao, Y.H. Matsuda, T.M. Pan, Structural and electrical characteristics of high-κ Er_2O_3 and Er_2TiO_5 gate dielectrics for a-IGZO thin-film transistors / Nanoscale Res. Lett. 8 (2013) 18. https://doi.org/10.1186/1556-276X-8-18

[9] L.P. Lyashenko, L.G. Shcherbakova, I.I. Tartakovskii, A.A. Maksimov, R.D. Svetogorov, Ya.V. Zubavichus, I.V. Kolbanev, Order-disorder structural transformations in highly imperfect fluorite-derived R_2TiO_5-based (R = Tm, Er) solid solutions, Inorg. Mater. 56 (2020) 190-197. https://doi.org/10.1134/S0020168520020119

[10] M.I. Samoylovich, A.F. Belyanin, A.S. Bagdasaryan, V. Bovtun, Structure and dielectric properties of nanocomposites: opal matrix - titanium oxide and rare-earth titanates, Fine Chem. Technol. 11 (2016) 66-73. https://doi.org/10.32362/2410-6593-2016-11-2-66-73

[11] M.I. Samoilovich, A.B. Rinkevich, V. Bovtun, A.F. Belyanin, M. Kempa, D. Nuzhnyy, M.Yu. Tsvetkov, S.M. Kleshcheva, Optical, magnetic, and dielectric properties of opal matrices with intersphere nanocavities filled with crystalline multiferroic, piezoelectric, and segnetoelectric materials, Rus. J. Gen. Chem. 83 (2013) 2132-2147. https://doi.org/10.1134/S1070363213110339

[12] P. Pooseekheaw, W. Thongpan, E. Kantarak, W. Sroila, T. Kumpika, P. Singjai, Effect of magnetic field on improvement of photocatalytic performance of V_2O_5/TiO_2 nanoheterostructure films prepared by sparking method, Sci. Rep. 12 (2022) 2298. https://doi.org/10.1038/s41598-022-05015-2

[13] G.C. Lau, B.G. Ueland, M.L. Dahlberg, R.S. Freitas, Q. Huang, H.W. Zandbergen, P. Schiffer, R.J. Cava, Structural disorder and properties of the stuffed pyrochlore Ho_2TiO_5, Phys. Rev. B. 76 (2007) 054430. https://doi.org/10.1103/PhysRevB.76.054430

[14] Yu.F. Shepelev, M.A. Petrova, Crystal structures of Ln_2TiO_5 (Ln = Gd, Dy) polymorphs, Inorg. Mater. 44 (2008) 1354-1361. https://doi.org/10.1134/S0020168508120170

[15] https://legacy.materialsproject.org/.

[16] A.B. Rinkevich, A.M. Burkhanov, M.I. Samoilovich, A.F. Belyanin, S.M. Kleshcheva, E.A. Kuznetsov, Three-dimensional nanocomposite metal dielectric materials on the basis of opal matrices, Rus. J. Gen. Chem. 83 (2013) 2148-2158. https://doi.org/10.1134/S1070363213110340

[17] S.T. Bramwell, M.N. Field, M.J. Harris, I.P. Parkin, Bulk magnetization of the heavy rare earth titanate pyrochlores - a series of model frustrated magnets, J. Phys.: Condens. Matter 12 (2000) 483-495. https://doi.org/10.1088/0953-8984/12/4/308

[18] G. Ehlers, J.S. Gardner, Y. Qiu, P. Fouquet, C.R. Wiebe, L. Balicas, H.D. Zhou, Dynamic spin correlations in stuffed spin ice $Ho_{2+x}Ti_{2-x}O_{7-\delta}$, Phys. Rev. B. 77 (2008) 052404. https://doi.org/10.1103/PhysRevB.77.052404

[19] R. Pohle, L.D.C. Jaubert, Curie-law crossover in spin liquids, Phys. Rev. B. 108 (2023) 024411. https://doi.org/10.1103/PhysRevB.108.024411

[20] V.V. Ustinov, A.B. Rinkevich, D.V. Perov, A.M. Burkhanov, M.I. Samoilovich, S.M. Kleshcheva, E.A. Kuznetsov, Giant antiresonance in electromagnetic wave reflection from a 3D structure with ferrite spinel nanoparticles, Tech. Phys. 58 (2013) 568-577. https://doi.org/10.1134/S1063784213040257

[21] R. Mayoral, J. Requena, C. Lypez, S.J. Moya, H. Mhguez, L. Vozquez, F. Meseguer, M. Holgado, A. Cintas, A. Blanco, 3D long-range ordering in an SiO_2 submicrometer-sphere sintered superstructures, Adv. Mater. 9 (1997) 257-260. https://doi.org/10.1002/adma.19970090318

[22] M.I. Strashnikova, E.V. Mozdor, Limits of applicability of the Kramers-Kronig relations in the presence of an additional light wave, J. Exp. Theor. Phys. 87 (1998) 756-763. https://doi.org/10.1134/1.558718

[23] A.B. Rinkevich, D.V. Perov, E.A. Kuznetsov, M.S. Stenina, Microwave dielectric permittivity of nanostructured RMn_2O_5 manganate, $R_2Ti_2O_7$ titanate, and $LiCoPO_4$ and $LiNi_{0.5}Co_{0.5}PO_4$ orthophosphate composites, Nanomaterials. 15 (2025) 995. https://doi.org/10.3390/nano15130995

[24] Y.A. Pakhomov, A.B. Rinkevich, D.V. Perov, A.F. Belyanin, E.A. Kuznetsov. Structure and Microwave Properties of Nanocomposites with Embedded Spinel Particles Subjected to High-Temperature Annealing, IEEE Transactions on Nanotechnology. 20 (2021) 449-458. https://doi.org/10.1109/TNANO.2021.3079170

https://doi.org/10.31875/2410-4701.2026.13.04